Caterpillar like motion of droplet in a shear flow

Antonio Chahine, Julien Sébilleau, R. Mathis, Dominique Legendre

Caterpillar like motion of droplet in a shear flow

A. Chahine, J. Sebilleau, R. Mathis, and D. Legendre

Institut de Mécanique des Fluides de Toulouse (IMFT),

Institut National Polytechnique de Toulouse,

2 Allée du Professeur Camille Soula, 31400 Toulouse, France

Abstract

This paper is devoted to a specific motion observed for glycerin droplets sliding on a horizontal hydrophobic substrate under the influence of a shear flow. In this regime, the droplet elongates in the flow direction, adopting a rivulet shape. Waves develop on the droplet sheared surface, resulting in a wavy contracting and stretching motion mechanism, similar to the movement of a caterpillar. If long enough, the droplet can break up into several droplets that can be submitted to a pearling instability. Furthermore, these droplets can also coalesce.

Keywords: Rivulet, Deformed Interface, Caterpillar

I. INTRODUCTION

Droplets sliding along a substrate under partial wetting conditions is a common phenomenon that can be observed on windshields and windows during rainy days. This sliding motion, that results from the effects of gravity [1–8], the drag exerted by an air flow [9–15], or by a combination of both effects [16–19], is of fundamental importance due to the remarkable richness of phenomena that arise. For a droplet sliding along an incline (i.e., under the effect of gravity), experimental studies [2, 3, 7] have reported three different droplet shapes: oval, corner, and cusp, depending on the droplet volume and velocity. These shapes have been retrieved with a theoretical model based on the long-wave approximation [4] with an additional rivulet shape where the droplet becomes very elongated and is thus similar to a rivulet. This rivulet shape has also been observed by Yang *et al.* [20] with a modified pseudopotential lattice Boltzmann multiphase model. This rivulet shape is different from the thin rivulet that forms at the receding contact line in the cusp regime [7], which can lead to a pearling instability [4, 5]. In the case of a droplet sliding onto a horizontal substrate in a shear flow, the droplet can adopt an oval, corner, or rivulet shape depending on its volume and velocity and on the shear flow [10–15]. The rivulet shape has been observed experimentally on aluminum [14] or glass substrates [15], and it has been observed that these rivulets eventually break into smaller droplets when long enough.

The present paper describes one particular kind of rivulets which we have observed: an extremely long droplet whose motion is induced by surface waves, inducing stretching and shrinking of the droplet interface, akin to a caterpillar. Surface waves on very long rivulets (corresponding to a Bond number Bo>4) have been previously observed by Yang *et al.* [20] in their numerical study of a droplet sliding along an incline. Nevertheless, they do not report any influence of these waves on the droplet motion. The only similar sliding regime described in the literature was briefly reported in Yurishchev *et al.* [19] for a water droplet motion climbing an incline under the shear of a turbulent flow. They have described the stretching and shrinking motion of a very long rivulet, but, as their paper was devoted to the mean droplet velocity, they did not provide any details on the physical mechanisms underlying this motion.

It should be emphasized that oscillations can appear in all sliding regimes in the case of a water droplet, as described by Chahine *et al.* [15], which makes it difficult to distinguish

between these mere oscillations to those responsible for the caterpillar motion. For such a reason, the present work was conducted with a glycerin droplet sliding on a horizontal substrate under a laminar shear flow, for which no oscillations were observed [15]. This much simpler configuration enables a better description of the caterpillar like motion, which results from surface waves that travel faster than the droplet.

In the next section (Sec. II), we first report observations of a shear driven glycerin droplet sliding on a glass substrate, exhibiting surface waves, and we identify flow and droplet conditions at which this phenomenon emerges. Next, we explore the characteristics of the surface waves (Sec. III), and then we investigate disorganizing events such as droplet breakup, pearling, and coalescence (Sec. IV). A summary and conclusions are provided in the last section (Sec. V).

II. CATERPILLAR LIKE MOTION OBSERVATION

This caterpillar like motion has been observed for glycerin droplets, of volume V_d ranging from 40 to 100 µL, sliding on a hydrophobic horizontal glass plate (with typical receding and advancing contact angles $\theta_r = 83°$ and $\theta_a = 86°$) induced by a laminar shear flow with a free-stream velocity $U_\infty = 20$ and 22 m/s. Two cameras were used to simultaneously record side and bottom views of the droplet during its motion. A more detailed description of the experimental setup is available in Ref. [15]. Figure 1 presents typical observed snapshots of a sliding glycerin droplet ($V_d = 60$ µL and $U_\infty = 22$ m/s).

Prior to the airflow application, the droplet is almost hemispheric. When increasing progressively the air flow, it first begins to tilt in the flow direction, exhibiting an oval shape. When the drag force exerted by the air-flow overcomes the capillary force, the droplet begins to slide (this onset of sliding has been investigated in our previous study [15]) and the shape passes through the corner and rivulet shapes. When the rivulet tail is long enough, waves develop on the droplet sheared surface inducing caterpillar like motion and eventually breakup (rivulet wave and rivulet breakup regimes). When reaching the advancing contact line, these surface waves induce a sudden acceleration which is responsible for the stretching and shrinking of the droplet, similarly to what can be observed in the movement of a caterpillar. It should be emphasized that in the following, several droplet

length scales are used to describe its evolution. First, its geometric form evolution over the time is described using the dimensionless length $\overline{L} = L/(2R_0)$, width $\overline{W} = W/(2R_0)$ and height $\overline{H} = H/(2R_0)$ where the characteristic length $R_0 = [3V_d/(2\pi)]^{1/3}$ is defined as the radius of the hemisphere of the same volume. This gives an insight into the evolution of the droplet in comparison with an idealized hemispherical shape, i.e., $\overline{L} = \overline{W} = \overline{H} = 1$. We also introduce the dimensionless length L/ℓ_c to compare the droplet length to the capillary length $\ell_c = \sqrt{\sigma/\rho_d g}$ (where σ is the droplet surface tension and ρ_d is the droplet density). We also consider in the following the critical droplet length L_{app}/ℓ_c at which the surface waves start to develop and the maximum length of the droplet, $L_{\max}/\ell_c$, prior to breaking.

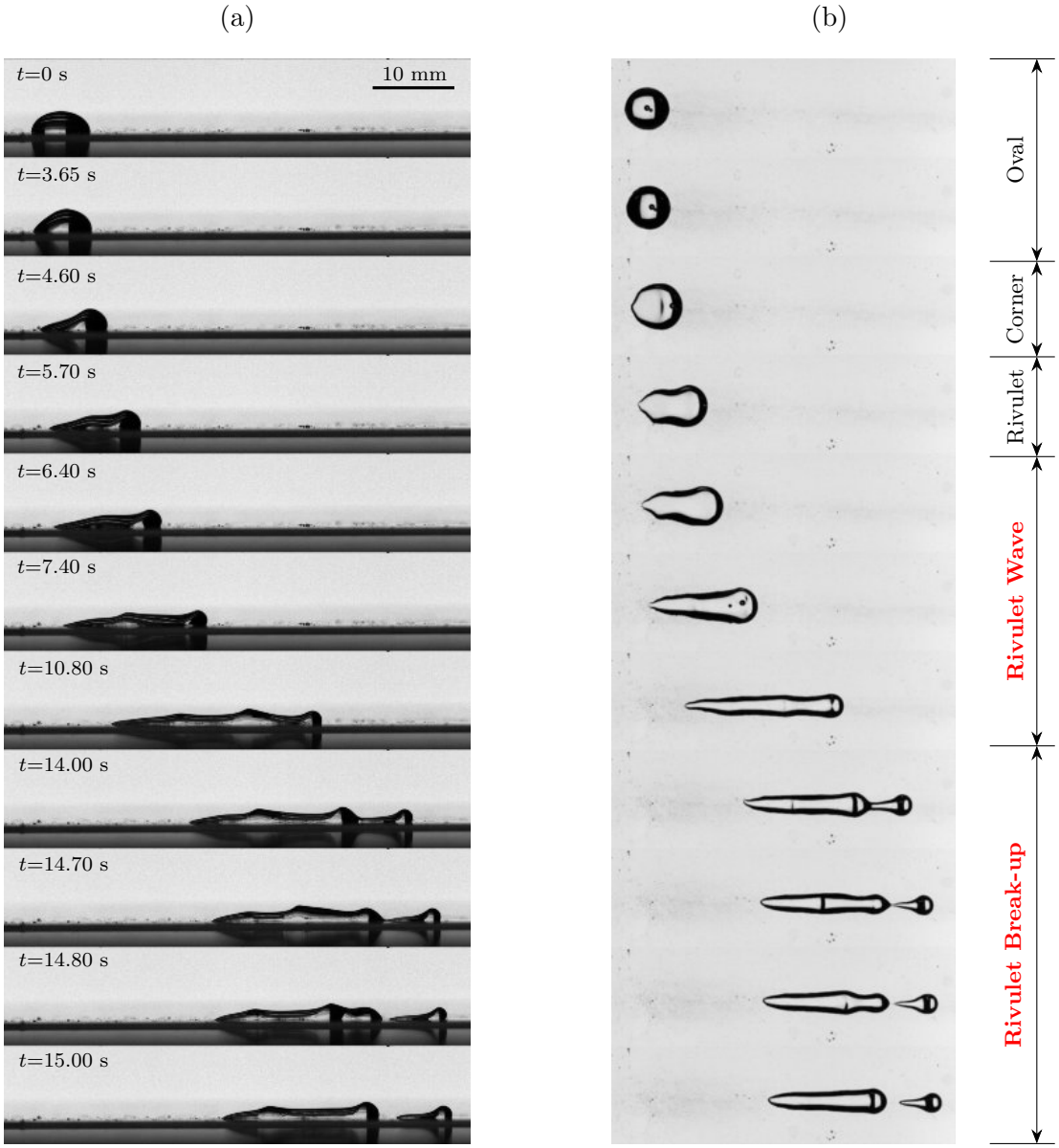

FIG. 1: (a) Side and (b) bottom views of a glycerol droplet sliding along a hydrophobic glass surface under the influence of a sheared airflow, V_d = 60 µL – U_∞ = 22 m/s.

Figure 2 presents the time evolution of several geometric parameters extracted from the video recordings for a glycerin droplet (V_d = 60 µL) in a laminar shear flow with U_∞ = 20 m/s, for which no rivulet breakup appears. Figure 2 (a) presents the advancing (downstream) X_a and receding (upstream) X_r contact line positions and Fig. 2 (b) presents the normalized width $\overline{W} = W/(2R_0)$, length $\overline{L} = L/(2R_0)$, and maximal height $\overline{H} = H/R_0$ of the droplet, where the characteristic length $R_0 = [3V_d/(2\pi)]^{1/3}$ is defined as the radius of the hemisphere

of the same volume.

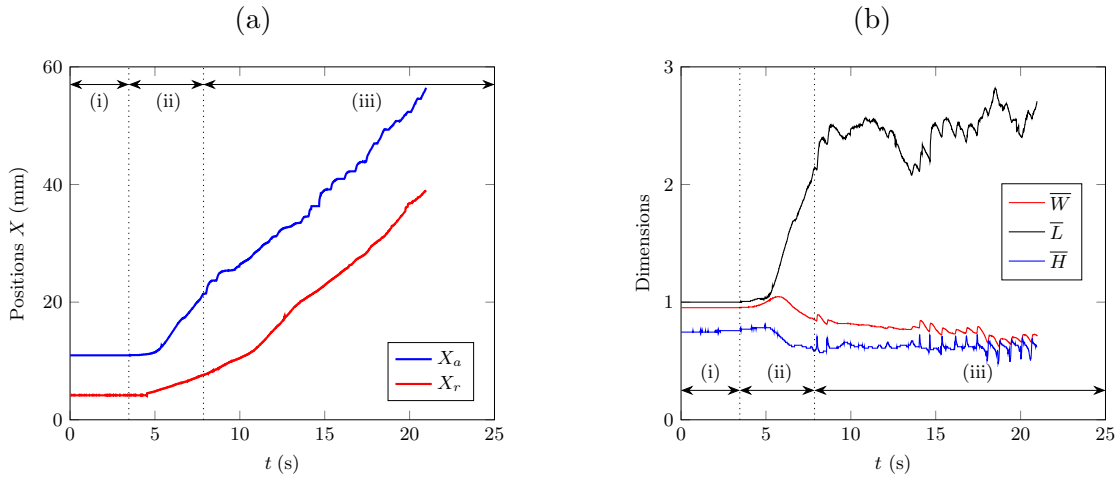

FIG. 2: Time evolution of (a) advancing (downstream) X_a and receding (upstream) X_r contact line positions of the droplet and (b) dimensionless width $\overline{W} = W/(2R_0)$, length $\overline{L} = L/(2R_0)$, and maximal height $\overline{H} = H/R_0$ of a glycerol droplet sliding on a hydrophobic glass surface under the influence of a sheared airflow, $V_d = 60$ µL and $U_\infty = 20$ m/s.

The droplet shape evolution appears to follow the same three stages observed by Yang *et al.* [20] in their numerical study in which they report surface waves on very long rivulets for a droplet sliding along an incline:

- (i) Relaxation: The droplet initially tilts and starts sliding in a small displacement because of the aerodynamic forces. We can see the characteristic sizes ($\overline{H}$, $\overline{L}$, $\overline{W}$) of the droplet remain almost constant [see Fig. 2 (b)].

- (ii) Stretch: The normalized length $\overline{L}$ increases while the normalized width $\overline{W}$ and height $\overline{H}$ both decrease with time. Due to the shear-induced drag force, the droplet stretches in the flow direction, resulting in different slopes for the advancing (X_a) and receding (X_r) contact line positions. This stretching continues until the droplet length $\overline{L}$ reaches a critical value much larger than the capillary length ℓ_c.

- (iii) Equilibrium: The droplet continues sliding at a constant speed while surface waves propagate inducing droplet oscillations that can eventually lead to a breakup of the droplet [see Fig. 2 (a)].

It is noticeable that the equilibrium stage (iii) appears when the droplet length reaches a critical value L_{app} which is approximately five times the capillary length ℓ_c for all droplet volumes as illustrated in Fig. 3.

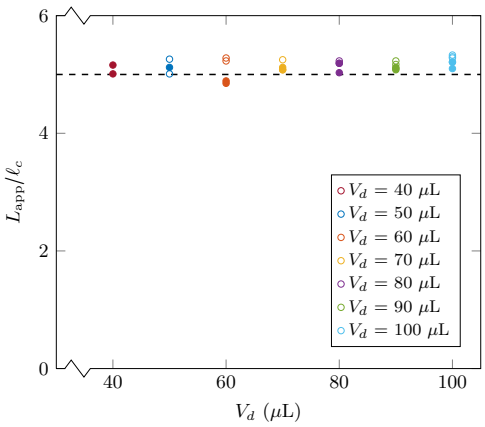

FIG. 3: Evolution of the ratio between caterpillar length at the beginning of the equilibrium stage (iii) (L_{app}) and capillary length (ℓ_c) for different volumes of the droplet. Open symbols indicate $U_\infty = 20$ m/s while solid symbols represent $U_\infty = 22$ m/s.

Furthermore, contrary to the observation of Yang *et al.* [20], the droplet velocity is not constant during its sliding, a consequence of the development of surface waves that play an important role on the droplet motion. This is illustrated in Fig. 4 (a) that presents the time evolution of the droplet's centroid X_c (computed from the side view). As one can see, in the equilibrium stage (that begins approximately 7 s after the application of the airflow) the centroid position begins to oscillate, which is clearly visible in Fig. 4 (a) for a time larger than 15 s. A cycle of this oscillatory motion is highlighted in the inset of Fig. 4 (a) and the corresponding side views of the droplet are given in Fig. 4 (b). During this cycle, the receding (downstream) contact line appears to move continuously during the wave propagation (from t_0 to t_3) but remains pinned while the wave reach the droplet's head (at t_3). On the contrary, the advancing (upstream) contact line stays pinned during almost all the cycle and moves only when the waves reaches the droplet's head (at t_3). Thus the droplet's length first contracts during the cycle and at t_3 stretches to recover its initial size as illustrated in Fig. 4 (b). This wavy contracting and stretching motion mechanism is closely similar to the movement of a caterpillar.

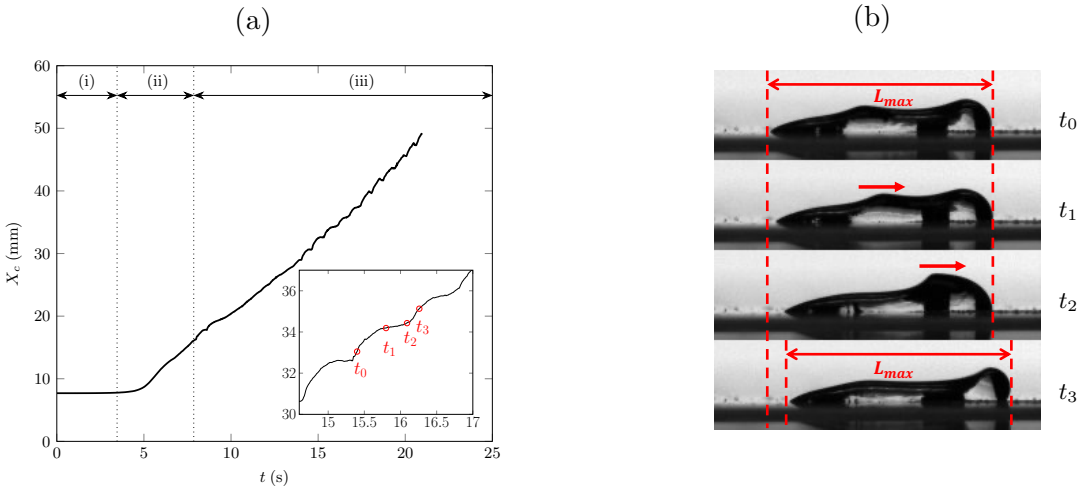

FIG. 4: (a) Time evolution of the centroid position X_c for a droplet of $V_d = 60$ μL and wind velocity of $U_\infty = 20$ m/s, and (b) one cycle of wave movement during the caterpillar droplet locomotion.

The time evolution of the advancing (upstream) and receding (downstream) contact angles are reported in Fig. 5 (a) during the caterpillar like motion. The raw data are presented in shaded color while the bold lines represent filtered data owing to a moving average filter. In the relaxation stage (i), the advancing contact angle remains almost constant while the receding contact angle decreases. In the stretching stage (ii), both the advancing and receding contact angles evolve: The receding contact angle continues to decrease while the advancing contact angle begins to oscillate. In the equilibrium stage (iii), the receding contact angle first reaches a minimum around 18° and then increases to reach a value about 28° while the advancing contact angle continues to oscillate. The contours presented in Fig. 5 (b) have been extracted from the side views of Fig. 4 (b) where the last one (at time t_3) has been shifted to have the same advancing contact line position to help the comparison. As one can see, the strong oscillations observed in the advancing contact angles are induced when the surface waves reach the droplet head, thus generating the caterpillar like motion.

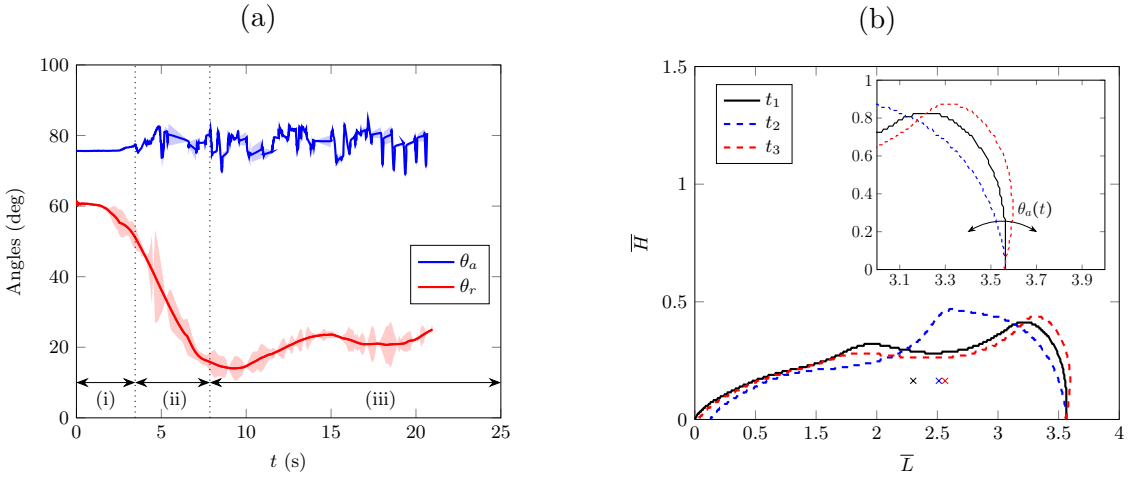

FIG. 5: (a) Time evolution of advancing and receding angles of a glycerol droplet sliding on a hydrophobic glass surface under the influence of a sheared airflow, $V_d = 60$ µL and $U_\infty = 20$ m/s and (b) dimensionless side view contours at the instants t_1, t_2, t_3 of Fig. 4 (b), where the symbol × marks the location of the droplet's centroid (X_c, Y_c).

III. WAVE PROPERTIES

It appears that the caterpillar like motion of the droplet is intimately linked to the propagation of waves on the droplet surface that is schematized in Fig. 6.

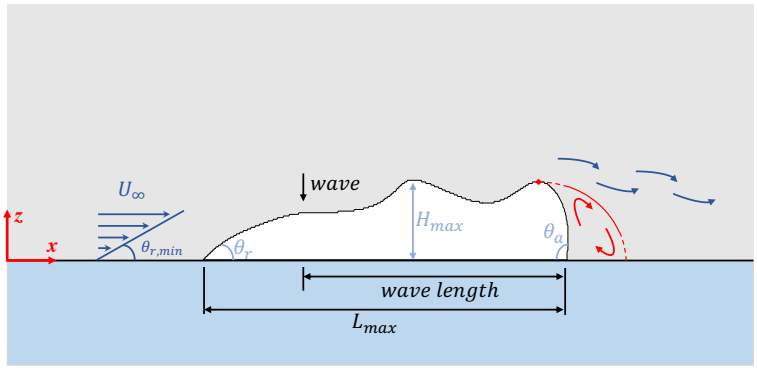

FIG. 6: The schematic of a two-dimensional (2D) caterpillar droplet on a glass surface, subject to the uniform air shear flow parallel to the substrate.

For all experiments, the number of wave cycles observed on the droplet sheared surface varies between 16 and 48, which allows the determination of their frequency f_w and velocity U_w presented in Figs. 7 and 8. Figure 7 (a) illustrates the temporal progression of the wind

tunnel velocity, wherein the initial oscillations are due to the controller of the wind tunnel speed. These oscillations have a typical frequency of 0.3 Hz, which is almost one order of magnitude lower than the droplet surface waves, as seen in Fig. 7 (b), and are thus considered to have a negligible influence on the droplet motion. The temporal evolution of the wave frequencies of droplets having the same volume is reported in Fig. 7 (b) for the two studied shear flows, U_∞ = 20 and 22 m/s. The dashed line represents a fitted curve made on all the data. We observe that the frequencies initially exhibit higher values and gradually decrease until they stabilize around a particular value. Once the wind tunnel velocity is stabilized, which occurs about 10 s as seen in Fig. 7 (a), the droplet wave frequency becomes constant, implying the establishment of a stable regime of the caterpillar motion.

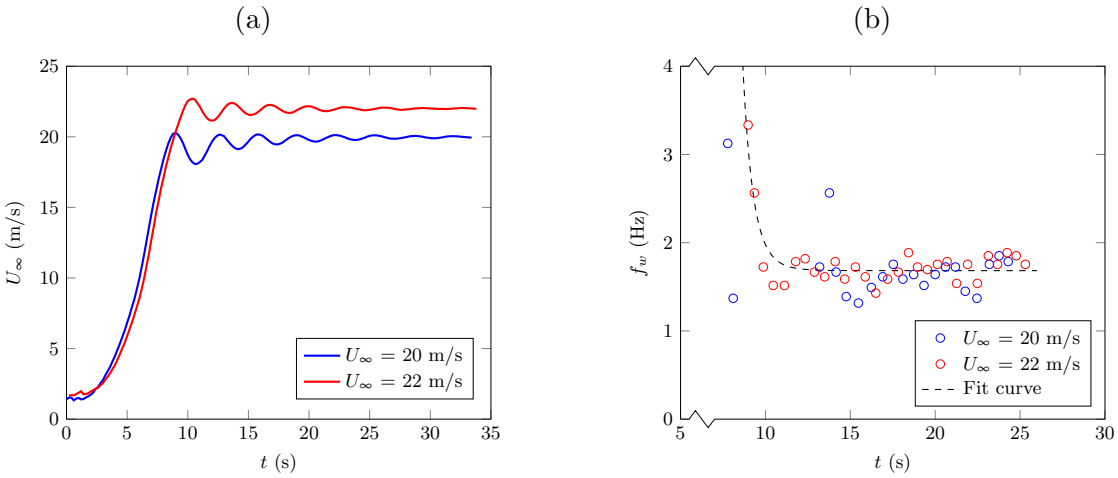

FIG. 7: Time evolution of (a) the airflow variation speed of the wind tunnel for U_∞ = 20 and 22 m/s and (b) the frequencies of the wave of glycerol droplet V_d = 60 µL. The dashed line is a fit curve realized on all the data.

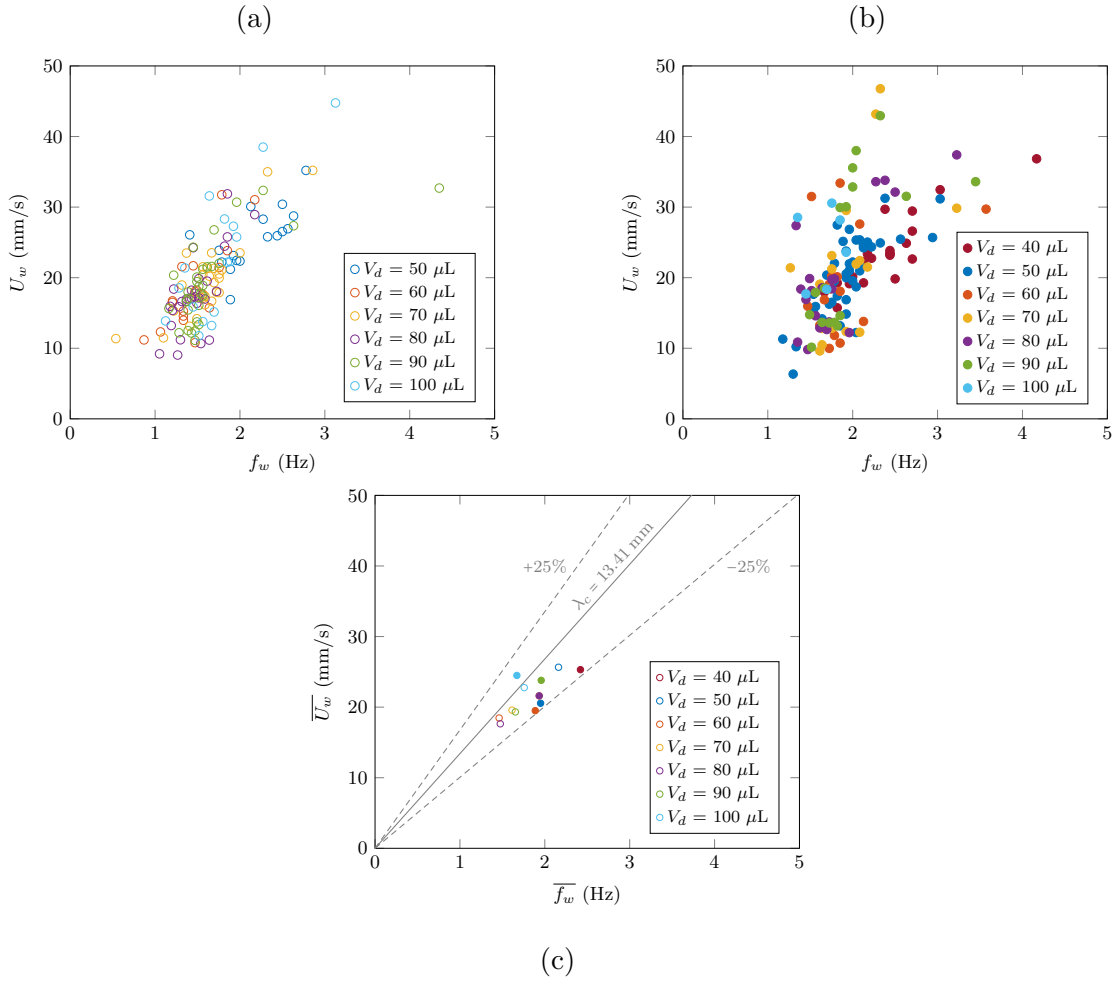

FIG. 8: The experimental frequencies and velocities of the interface wave on the droplet. (a) $U_\infty = 20$ m/s, (b) $U_\infty = 22$ m/s and (c) The mean values of the frequencies and velocities measured in each droplet: The continuous line reports the gravity-capillary wavelength $\lambda_c = 2\pi\ell_c$. Open symbols: $U_\infty = 20$ m/s; solid symbol: $U_\infty = 22$ m/s.

TABLE I: Mean wave frequency, velocity, and wavelength of glycerol droplets for different volumes, initial conditions, and wind velocities. The variables marked with an overbar are the mean values, and Std is the standard deviation.

U_∞ (m/s)	V_d (μL)	$\overline{f_w}$ (Hz)	$Std(f_w)$	$\overline{U_w}$ (m/s)	$Std(U_w)$	$\overline{\lambda_w}/\lambda_c$
20	50	2.08	0.376	0.026	0.0043	0.932
	60	1.46	0.307	0.018	0.0060	0.917
	70	1.61	0.393	0.020	0.0055	0.924
	80	1.47	0.244	0.018	0.0055	0.910
	90	1.63	0.586	0.019	0.0060	0.865
	100	1.73	0.460	0.023	0.0095	0.992
22	40	2.49	0.435	0.025	0.0048	0.746
	50	1.95	0.346	0.021	0.0054	0.805
	60	1.88	0.480	0.020	0.0074	0.790
	70	1.93	0.421	0.022	0.0104	0.850
	80	1.87	0.472	0.022	0.0083	0.880
	90	1.95	0.486	0.024	0.0110	0.917
	100	1.59	0.270	0.024	0.0051	1.126

To analyze further this regime, the mean wave frequency and mean velocity of the droplet of all experiments are reported in a phase diagram given in Fig. 8, and summarized in Table I with the corresponding wavelength normalized by the gravity-capillary wavelength [21]:

$$\lambda_c = 2\pi\ell_c = 2\pi\left(\frac{\sigma}{\rho g}\right)^{\frac{1}{2}}. \tag{1}$$

The caterpillar wavelength appears to be close to the gravity-capillary wavelength, but its wave velocity, $\overline{U_w} \approx 18$ mm/s, is found to be one order of magnitude smaller than the capillary-gravity wave velocity:

$$U_c = \sqrt{2}\left(\frac{g\sigma}{\rho}\right)^{\frac{1}{4}} \approx 200 \text{ mm/s}. \tag{2}$$

It is noticeable that the caterpillar waves show similarities with solitary waves observed in falling films [22, 23]. According to Chang [23], the velocity of solitary waves is about

three times the mean velocity of the liquid film and follows the amplitude-speed correlation of the form

$$c - 3 = 3\,(h - 1)\,, \tag{3}$$

where c is the ratio of the wave velocity to the mean film velocity and h is the ratio of the wave amplitude to the mean film height. By making the analogy between free-surface solitary waves and the observed caterpillar motion, $\overline{U_{sw}}$, directly from the mean droplet velocity U_d,

$$\overline{U_{sw}} = 3hU_d. \tag{4}$$

In order to test this relationship, we can evaluate the right-hand side of Eq. (4), by estimating the droplet velocity at its centroid, leading to $U_d \approx 5$ mm/s, and by taking h as the ratio of the maximum droplet's height prior to the wave appearance H_{max} [i.e., at the transition between phases (ii) and (iii)] to the amplitude of the wave H_d, which leads to

$$h = \frac{H_{max}}{H_d} \approx 1.25. \tag{5}$$

Thus, Eq. (4) leads to an estimate of the wave velocity $\overline{U_{sw}} \approx 18.8$ mm/s, which is very close to our experimental measured value $\overline{U_w} \approx 18$ mm/s. This analogy with a liquid film wave is reinforced by plotting in Fig. 9 the evolution of the ratio between the measured wave velocity $\overline{U_w}$ and $h\overline{U_d}$ for all our experiments. The plot confirms that the wave velocity at the interface of the caterpillar droplet is proportional to three times the velocity of the droplet, regardless of both the droplet volume or airflow considered. Solitary waves have been observed in falling liquid films at a relatively large Reynolds numbers (Re > 50), due to the destabilizing and dispersive effects of liquid inertia [23]. The effect of an additional shear stress on the long waves propagating on a falling film has been studied by Samanta [24]. He has shown that when an imposed shear stress is exerted downstream, the long waves appear at a smaller Reynolds number and grow faster. In our study, the Reynolds number of the droplets is very low (Re < 10^{-2}) but the Reynolds number of the air flow at the droplet surface (based on the droplet height H_d and the flow velocity at the same height estimated from the Blasius boundary layer profile) is rather high, Re = $\frac{\rho_a U_H H_d}{\mu_a} \approx 3 \times 10^3$ and the airflow provides the necessary inertia to the droplet interface to trigger the surface waves.

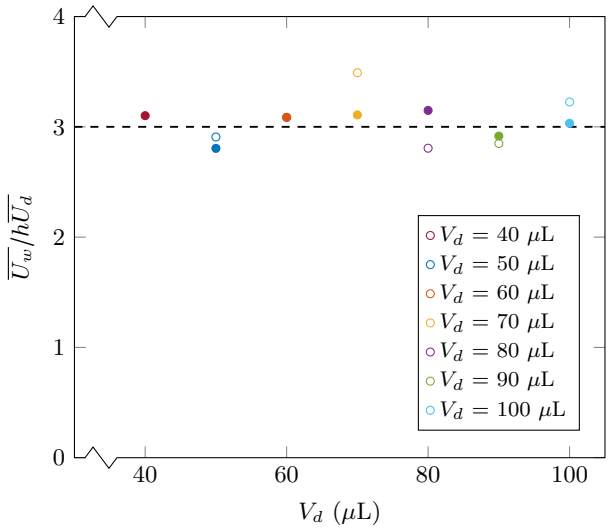

FIG. 9: Evolution of the ratio between mean wave velocity $\overline{U_w}$ and droplet mean velocity $\overline{U_d}$ times the dimensionless height h for different droplet volumes and airflow rates.

IV. BREAKUP, PEARLING, AND COALESCENCE

During the equilibrium stage, when the droplet is long enough, the droplet exhibits a caterpillar like motion during several tens of surface wave cycles before breaking into several smaller droplets (that can further coalesce). Sometimes, a pearling instability occurs at the receding contact line similar to the case of a droplet sliding on an incline. This behavior is illustrated in Fig. 10, which presents for the two shear flows the time evolution of the droplet length (L) over the capillary length (ℓ_c) on the left-hand side, and three characteristic snapshots of the caterpillar behavior on the right-hand side.

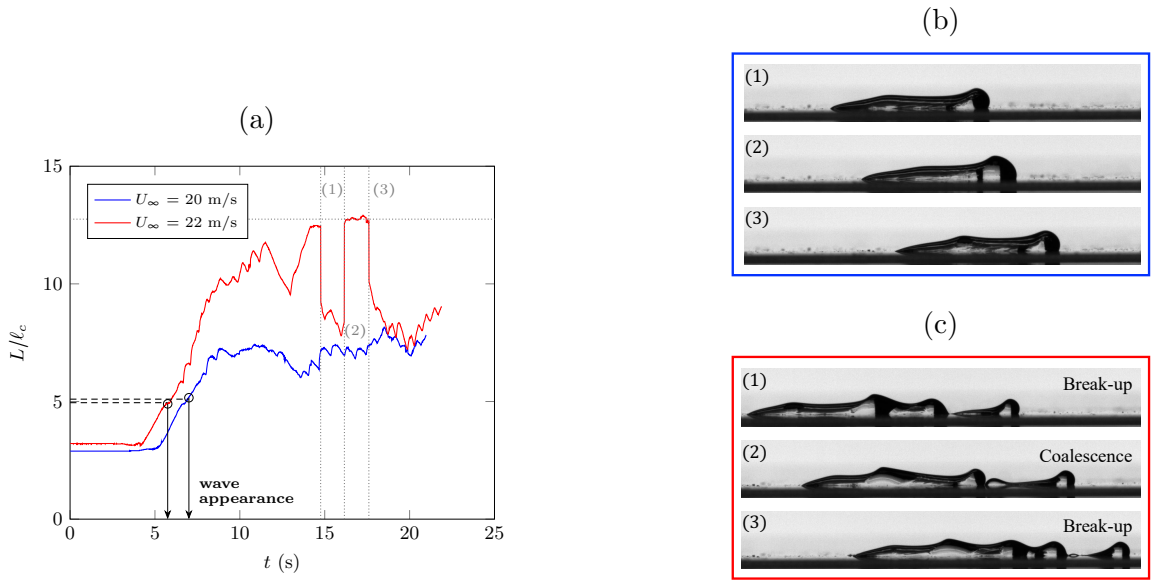

FIG. 10: (a) Time evolution of the dimensionalized length over the capillary length of a glycerol droplet sliding on a hydrophobic glass surface under the influence of a sheared airflow, $V_d = 60$ µL. Different images of the glycerol droplet at three different instants, (b) $U_\infty = 20$ m/s and (c) $U_\infty = 22$ m/s, where in this case (1) and (3) show a droplet breakup, whereas (2) depicts a droplet coalescence.

For a free-stream velocity of U_∞ = 20 m/s we can observe in the equilibrium stage (beyond 10 s) for a droplet's volume V_d = 60 µL a typical caterpillar wave motion with a droplet length oscillating between six to eight times the capillary length [see Fig. 10 (a)] and waves propagating at the droplet's surface [see Fig. 10 (b)]. By increasing the free-stream velocity just by 10%, up to U_∞ = 22 m/s for the same droplet's volume V_d = 60 µL, there is a stark contrast in the caterpillar behavior with a succession of breakup and coalescence stages [noted (1) (3) in Fig. 10]. When the length of the droplet is approximately five times larger than the capillary length ($L/\ell_c \approx 5$), we observe the evident emergence of the free wave, as depicted in Fig. 10 (a).

Furthermore, if the droplets created after the breakup exhibit a rivulet shape, pearling instability may appear. The length of the caterpillar and the number N_d of daughter droplets created after breakup, as well as the occurrence or not of coalescence and pearling phenomena, are reported in Table II and in the phase diagram $L_{\max}/\ell_c$ - N_d shown in Fig. 11, with $L_{\max}$ the maximum length that the droplet achieved before it breaks. As one can see,

breakups occur only for sufficiently long caterpillars. There is no breakup, i.e., N_d = 1, for droplets shorter than 12 times the capillary length ℓ_c. It is noticeable that breakup occurs only from droplets larger than two mean wavelength λ_c, which appears natural as the breakup appears to be linked to a wave interaction on the droplet sheared surface. The number of daughter droplets N_d is clearly increasing with the droplet's length, which also appears natural as a longer droplet can then exhibit more waves on its free surface. It should be noted that $L_{\max}$ appears to be set by the initial volume of the droplet and the wind speed, as seen in Table II. Also, the same initial conditions (droplet volume and wind speed) do not always necessarily produce the same results, with variability in $L_{\max}$ and N_d, which suggests that other underpinning processes should be considered.

TABLE II: Maximum length ($L_{\max}$) over the capillary length (ℓ_c) of a glycerol droplet for different airflow velocities and droplet volumes before it starts to divide into N_d daugther droplets.

U_∞ (m/s)	V_d (µL)	$L_{\max}/\ell_c$	N_d	Observed Phenomena
20	90	13.21	2	Coalescence/Pearling
	100	15.60	2	Coalescence/Pearling
	100	25.41	4	Coalescence/Pearling
	100	25.50	4	Coalescence/Pearling
22	60	12.75	2	Coalescence
	70	13.62	2	Coalescence
	70	15.62	3	Coalescence/Pearling
	80	15.71	3	Coalescence/Pearling
	80	16.71	3	Coalescence/Pearling
	90	19.05	3	Coalescence/Pearling
	90	24.03	3	Coalescence/Pearling
	100	22.04	4	Coalescence/Pearling
	100	22.29	4	Coalescence/Pearling

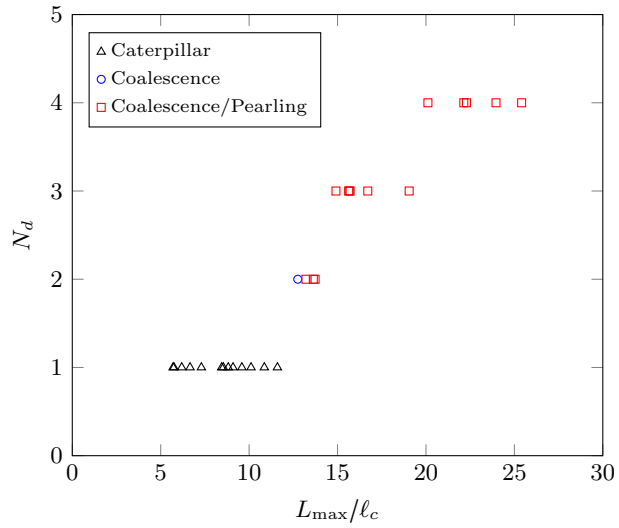

FIG. 11: Phase diagram $L_{\max}/\ell_c$ - N_d reporting the different observed behaviors. N_d = 1 indicates that the droplet is not experiencing any breakup.

Side view snapshots of the longest droplet observed before breakup, for V_d = 100 μL and U_∞ = 20 m/s, are reported in Fig. 12. Just before the breakup, at 13.75 s, this droplet has reached a maximal length of seven times its initial length, more than 25 times the capillary length. Then, the droplet breaks into four daughter droplets, where it is seen that the first three droplets in the line are much smaller than the last one. Evidence of pearling instability is also observed in the three primary daughter droplets.

There is an interesting interaction that can be observed between the mother droplet and the first downstream daughter droplet. The latter, marked with a red arrow in Fig. 12, appears to move in the opposite direction of the air flow towards the mother droplet, and eventually coalesces with it. This specific motion can be related to a back flow region developing downstream of the rivulet droplet presenting a caterpillar like motion. Such a back flow region is linked to a vortex shedding that has been previously reported in the case of small droplets using particle image velocimetry (PIV) measurements [12] and is similar to the hairpin vortex generated by a hemisphere in a laminar boundary layer [25]. A similar phenomenon was also reported for droplets in the wake of a hemisphere by Hooshanginejad *et al.* [26]. We measured the ratio of the mother droplet height h to the distance d between the mother droplet head and the daughter droplet tail, h/d = 0.29, which is found to be similar to the 0.33 value found by Zhang *et al.* [27] for a 3D droplet (the Reynolds number based on the droplet height being Re_H = 2070 in their study and Re_H = 1538 in our case).

These results appear consistent and validate the role of the back flow in such coalescence events.

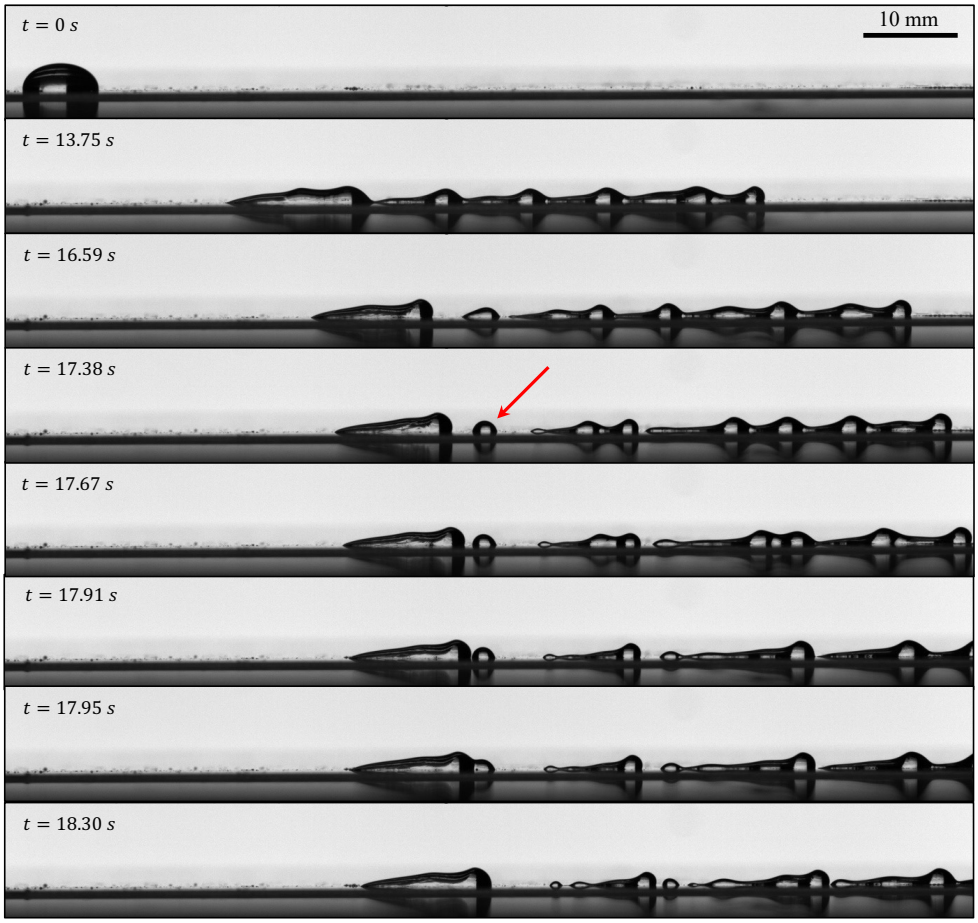

FIG. 12: Side views of a line of daughter glycerol droplets sliding from left to right along a hydrophobic glass surface under the influence of a laminar shear airflow. The red arrow indicates the small droplet that is absorbed by the last droplet on the left after coalescence. V_d = 100 μL – U_∞ = 20 m/s.

V. CONCLUSION

In this study, caterpillar like motion of glycerin droplets in a laminar boundary layer is reported. It appears that the droplet is stretched by the airflow and eventually exhibits a long rivulet shape. Shear driven waves develop at the droplet interface and induce a caterpillar like motion that can eventually breakup into smaller droplets. These droplets can be subject to pearling instability and coalesce. The shear driven waves responsible for this caterpillar

like motion are well described by the Nusselt theory of waves developing on a flowing liquid film. When long enough (approximately two wavelengths), several waves develop on the droplet sheared surface and lead to droplet breakup and the number of daughter droplets increases with the droplet length. Finally, droplets moving in the opposite direction of the shear flow are also reported and appear to be linked to the backflow region that develops downstream the droplet.

---

[1] E. B. Dussan and R. Chow, "On the ability of drops or bubbles to stick to non-horizontal surfaces of solids," Journal of Fluid Mechanics **137**, 1–29 (1983).

[2] Podgorski, T. and Flesselles, J. M. and Limat, L., "Corners, cusps, and pearls in running drops," Physical Review Letters **87**, 361021–361024 (2001).

[3] Nolwenn Le Grand, Adrian Daerr, and Laurent Limat, "Shape and motion of drops sliding down an inclined plane," Journal of Fluid Mechanics **541**, 293–315 (2005).

[4] L. W. Schwartz, D. Roux, and J. J. Cooper-White, "On the shapes of droplets that are sliding on a vertical wall," Physica D: Nonlinear Phenomena **209**, 236–244 (2005).

[5] Jacco H. Snoeijer, N. Le Grand, L. Limat, H. A. Stone, and J. Eggers, "Cornered drops and rivulets," Physics of Fluids **19** (2007), 10.1063/1.2722767.

[6] Jean Baptiste Dupont and Dominique Legendre, "Numerical simulation of static and sliding drop with contact angle hysteresis," Journal of Computational Physics **229**, 2453–2478 (2010).

[7] Baburaj A. Puthenveettil, Vijaya K. Senthilkumar, and E. J. Hopfinger, "Motion of drops on inclined surfaces in the inertial regime," Journal of Fluid Mechanics **726**, 26–61 (2013).

[8] Ahmed Gulraiz, Sellier Mathieu, Jermy Mark, and Taylor Michael, "Modeling the effects of contact angle hysteresis on the sliding of droplets down inclined surfaces," European Journal of Mechanics - B/Fluids **48**, 218–230 (2014).

[9] E. B. Dussan, "On the ability of drops to stick to surfaces of solids. part 3. the influences of the motion of the surrounding fluid on dislodging drops," Journal of Fluid Mechanics **174**, 381–397 (1987).

[10] J. Fan, M. C.T. Wilson, and N. Kapur, "Displacement of liquid droplets on a surface by a shearing air flow," Journal of Colloid and Interface Science **356**, 286–292 (2011).

[11] S. Moghtadernejad, M. Mohammadi, M. Jadidi, M. Tembely, and A. Dolatabadi, "Shear Driven Droplet Shedding on Surfaces with Various Wettabilities," SAE International Journal of Aerospace **6** (2013), 10.4271/2013-01-2176.

[12] Liqun Ma, Yang Liu, and Hui Hu, "An experimental investigation on wind driven droplet moving on surfaces with different wettabilities," AIAA Scitech 2019 Forum (2019), 10.2514/6.2019-0632.

[13] Beawer Barwari, Sebastian Burgmann, and Uwe Janoske, "Hydrodynamic Instabilities of Adhering Droplets Due to a Shear Flow in a Rectangular Channel," Chemie Ingenieur Technik **91**, 991–1000 (2019).

[14] Shuoshuo Wang, Shinan Chang, Huanyu Zhao, and Chen Yang, "Dynamic behaviors of water droplet moving on surfaces with different wettability driven by airflow," International Journal of Multiphase Flow **154**, 104127 (2022).

[15] A. Chahine, J. Sebilleau, R. Mathis, and D. Legendre, "Sliding droplets in a laminar or turbulent boundary layer," Phys. Rev. Fluids **7**, 113605 (2022).

[16] A. J.B. Milne and A. Amirfazli, "Drop shedding by shear flow for hydrophilic to superhydrophobic surfaces," Langmuir **25**, 14155–14164 (2009).

[17] Edward B. White and Jason A. Schmucker, "Wind- and gravity-forced drop depinning," Phys. Rev. Fluids **6**, 023601 (2021).

[18] Alireza Hooshanginejad and Sungyon Lee, "Dynamics of a partially wetting droplet under wind and gravity," Physical Review Fluids **7**, 033601 (2022).

[19] Alexander Yurishchev, Amos Ullmann, and Neima Brauner, "Experiments and modeling of droplets motion induced by turbulent air flow on inclined surfaces," Experimental Thermal and Fluid Science **140**, 110763 (2023).

[20] Jiapei Yang, Xiao Ma, Linlin Fei, Xiaoqing Zhang, Kai H. Luo, and Shijin Shuai, "Effects of hysteresis window on contact angle hysteresis behaviour at large Bond number," Journal of Colloid and Interface Science **566**, 327–337 (2020).

[21] H. Lamb, *Hydrodynamics*, 6th ed. (Cambridge University Press, Cambridge, UK, 1993).

[22] W. Nusselt, "Die obserflachenkondensation des wasserdampfes," Z. Ver. Dtsch. Ing **60**, 541–546 (1916).

[23] H Chang, "Wave evolution on a falling film," Annual Review of Fluid Mechanics **26**, 103–136 (1994).

[24] Arghya Samanta, "Shear-imposed falling film," Journal of Fluid Mechanics **753**, 131–149 (2014).

[25] M. S. Acarlar and C. R. Smith, "A study of hairpin vortices in a laminar boundary layer. Part 1. Hairpin vortices generated by a hemisphere protuberance," Journal of Fluid Mechanics **175**, 1–41 (1987).

[26] Alireza Hooshanginejad and Sungyon Lee, "Droplet depinning in a wake," Phys. Rev. Fluids **2**, 031601 (2017).

[27] Xueqing Zhang, Burak A. Tuna, Serhiy Yarusevych, and Sean D. Peterson, "Flow development over isolated droplet-inspired shapes," International Journal of Heat and Fluid Flow **88**, 108756 (2021).